INSTITUT DE FRANCE
Académie des sciences

Comptes Rendus

Physique

Fernando Albarracin-Vargas, Felix Vega, Chaouki Kasmi, David Martinez and Lars Ole Fichte

Enhanced integrated multiband HPM radiator, combining a hyperband source with a high-Q frequency selective surface

Volume 22, Special Issue S1 (2021), p. 73-82

Published online: 6 May 2021
Issue date: 30 June 2021

https://doi.org/10.5802/crphys.63

Part of Special Issue: URSI-France 2020 Workshop
Guest editor: Joe Wiart (LTCI, Télécom Paris, Institut Polytechnique de Paris, Institut Mines-Télécom, France)

CENTRE MERSENNE

Les Comptes Rendus. Physique *sont membres du Centre Mersenne pour l'édition scientifique ouverte*
www.centre-mersenne.org
e-ISSN : 1878-1535

Comptes Rendus
Physique
2021, 22, nº S1, p. 73-82
https://doi.org/10.5802/crphys.63

URSI-France 2020 Workshop / *Journées URSI-France 2020*

Enhanced integrated multiband HPM radiator, combining a hyperband source with a high-Q frequency selective surface

Fernando Albarracin-Vargas [*, a], **Felix Vega** [a, b], **Chaouki Kasmi** [a, c], **David Martinez** [a] **and Lars Ole Fichte** [c]

[a] Directed Energy Research Centre, Technology Innovation Institute, Abu Dhabi, UAE

[b] Universidad Nacional de Colombia, Facultad de Ingenieria, Sede Bogota, Colombia

[c] Faculty of Electrical Engineering, Helmut Schmidt University, Germany

E-mails: fernando.albarracin@derc.tii.ae (F. Albarracin-Vargas), felix.vega@derc.tii.ae (F. Vega), chaouki.kasmi@derc.tii.ae (C. Kasmi), david.martinez@derc.tii.ae (D. Martinez), lo.fichte@hsu-hh.de (L. O. Fichte)

Abstract. This work presents advances on the development of a resonant radiator, obtained as the augmentation of a conventional Impulse Radiating Antenna (IRA) with a Frequency Selective Surface (FSS), in the L-band. An improved passband-type FSS is obtained by exploring the Multiple Split Ring Resonators (MCSRR) unit cells to obtain a higher *Q*-factor radiator. The effects of a multiband and of a tunable FSS's are also studied and verified via simulations. A variety of applications are enabled by modifying the UWB waveform from the IRA into a damped sinusoidal from the combined radiator like IEMI testing, hardening of infrastructures, cloaking of wide aperture radiators, among other. The system analysis methodology can also be applied to other FSS geometries, or the combinations of various of them.

Keywords. Frequency selective surface, Complementary split ring resonators, Electromagnetic hardening, Hyperband radiators, HPM sources, IEMI.

Available online 6th May 2021

1. Introduction

Design and development of hardening modules for critical infrastructures like airports, electrical grids, and IT headquarters involve the study of the Electromagnetic Compatibility (EMC), and Intentional Electromagnetic Interference (IEMI) effects. IEMI studies requires the characterization of potential disruptions on modern microelectronic systems. Such characterization require the use of high-power electromagnetic radiators consisting, in general, of complex, high-cost generators and sophisticated antennas [1, 2]. The task becomes even more challenging when tunable, band-pass, high power emitters are required to asses the radiated susceptibility of equipment and systems.

* Corresponding author.

A key part of the design of a pulse radiator is the antenna system. This involves the use of radiators with the ability to radiate at low frequency, nearly constant gain and impedance over bandwidth ratios greater than 10 (i.e., hyperband region), and high-voltage handling capabilities. The Impulse Radiating Antenna (IRA), first proposed by Baum and Farr [3, 4], is one of the most known radiators used in IEMI tests, due to its hyper-band response and high-voltage capability. The working principle of an IRA is to launch a spherical and non-dispersive TEM wave-front from the focal point of a parabolic reflector. Such a TEM spherical wave propagates through the feeder arms, that act as a TEM transmission line.

Both components mentioned so far, the antenna and the pulsed source, share two important characteristics: high cost and fixed working bandwidth. In this context, the use of a frequency selective planar structure arises as a strategy to add frequency agility to the system: Antenna + HPM source. The ability to radiate over multiple bands is possible by arranging multiple resonating unit-cell types into the Frequency Selective Surface (FSS), or by changing the separation of a multilayer lattice.

In related studies, it has been shown that a metal-grid embedded within the walls of a building displays interesting properties when illuminated with an ultra-wideband (UWB) radiator. Tesche *et al.* [5] analyzed the possibility of damping the emitted pulse signal by chaining a set of metal grids placed in front of the antenna. These serve to transform the fast-pseudo-impulse from the antenna into a damped sinusoidal waveform. A low-pass FSS that can be integrated into an ultra-wideband radiator was presented in [6]. Other alternatives, like the use of self-actuated surfaces, using arrays of semiconductors, are described in [7, 8]. A Voltage-controlled piezoelectric actuators are used to tune an FSS in [9].

Modern technologies, like the fifth generation (5G) wireless communication, can also take advantage of radiators enhanced with FSS's. On one hand, specific IEMI studies on systems in the sub-1 GHz band supporting Internet of things (IoT) platforms, and in the sub-6 GHz band used for handheld devices communications, are enabled because of the electrically small size of the resonant unit cells commonly implemented in FSS's. This condition allows developing manageable FSS's to conduct those tests. On the other hand, for higher frequency band services (i.e. 26 GHz band and beyond), where the multiple beam and massive MIMO capabilities are intended, radiators integrated with FSS's have been reported in [10]), in the form of pass-band radomes that prevent the transceiver from IEMI effects at frequencies other than the working ones.

FSS's are narrowband passive structures that exhibit interesting properties when illuminated by electromagnetic fields [11]. The well-known Split Ring Resonators (SRR) proposed in [12], and its complementary version (i.e., CSRR), have been studied and characterized in the last years as a compact structure to compose an FSS [13, 14]. To avoid diffractive effects and grating-lobes on the intended radiated beam, both the unit cell size and separation must be smaller than the wavelength of the incident radiation.

A relevant characteristic of these resonators is the capability of being cross-polarized. In an SRR, a polarizing surface results by either the E- or the H-field passing through the structure. This phenomenon produces a band-stop response [13]. On the other hand, an electric dipole is induced from the excitation of a CSRR with an incident wave whose electric field component is parallel to the rings' gaps, resulting in a bandpass filtering surface. Marques *et al.* [13] presented an analytical solution for the behavior of FSS based on SRR and CSRR cells. Although restricted to the infinitesimally thin perfect conductor in free space, the analytical approach gives a first approximation to the response of a band-pass-type FSS. Bilotti *et al.* proposed an approximation to the analytical model of Multiple-SRR (MCSRR) and Spiral Resonators in [15].

In this work, we explore a concept that can be used when a high-amplitude adjustable and high Q-factor band-pass electric field is required. The resulting integrated multiband and tunable

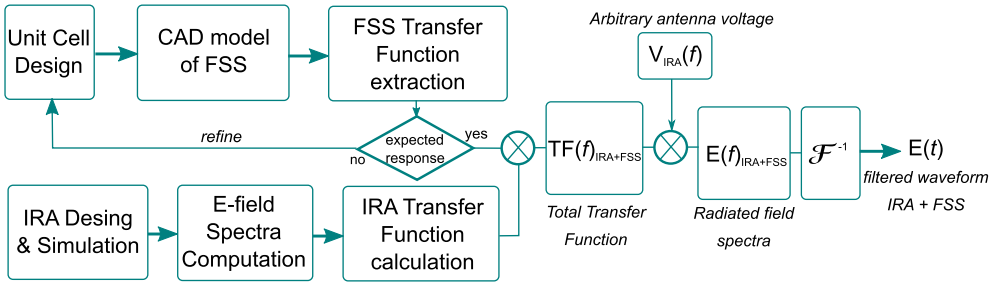

Figure 1. Design flowchart of the proposed integrated HPM radiator.

HPM radiators, are composed of a CSRR-based FSS in the near-field of a hyperband radiator, like the IRA. All the designs presented comprise a strategy to add waveform and frequency agility to the resulting HPM source. An improved version of the passband FSS is presented as the implementation of a Multiple-CSRR (MCSRR) instead of the conventional CSRR to obtain higher Q-factor response. The enhanced single-band and the multiband integrated HPM source approach, and the unit cell designs are described in Section 2. The cascaded-system analysis of the integrated radiator is presented in Section 3. Conclusions are included in Section 4.

2. Multiband and enhanced Q-factor FSS

In this section, we present an application of the proposed approach as the design of the FSS to be integrated with the IRA. The complete design methodology can be summarized in the scheme shown in Figure 1. The unit cell is designed and its CAD model is simulated as a periodic structure to obtain the S-parameter matrix of the FSS. A transfer function can be extracted by computing a representation of the electric and magnetic fields as voltage and current driving a two-port ABCD parameter set. A *total* transfer function is obtained as the product of the FSS transfer function and the transfer function from the IRA, which relates the radiated electric field with the voltage driving the antenna. Finally, the radiated electric field from the integrated HPM radiator can be computed, for any voltage waveform driving the IRA.

Two examples are presented as passband FSS's. The first one is a single layer FSS based on a conventional two-slots CSRR augmented with an additional pair of rings. A second FSS design incorporates of a second CSRR of different size to implement a multiband FSS whose passing bands are tuned around 1.5 GHz and 2.4 GHz, respectively.

2.1. *Single frequency CSRR, and MCSRR design*

Figure 2a shows the CSRR unit cell, inspired by [14], used to illustrate the single band FSS tuned at $f_0 = 1.5$ GHz. The circuit model of the unit cell is shown Figure 2b. As an alternative to enhance the selectivity of the passband FSS, a modified unit cell based on the multiple complementary ring resonators (MCSRR) is designed. The new geometry is sketched in Figure 2c, and its associated circuit model is shown in Figure 2d. The reactive parameters of the circuit models shown in Figures 2b,d, can be computed as [15, 16]:

$$\begin{aligned} L_0 &= (\mu_0/4\varepsilon_0)C_{0,\mathrm{SRR}} \\ C_c &= 4(\varepsilon_0/\mu_0)L_s \\ f_0 &= \frac{1}{2\pi}\sqrt{\frac{1}{L_c C_c}} \end{aligned} \tag{1}$$

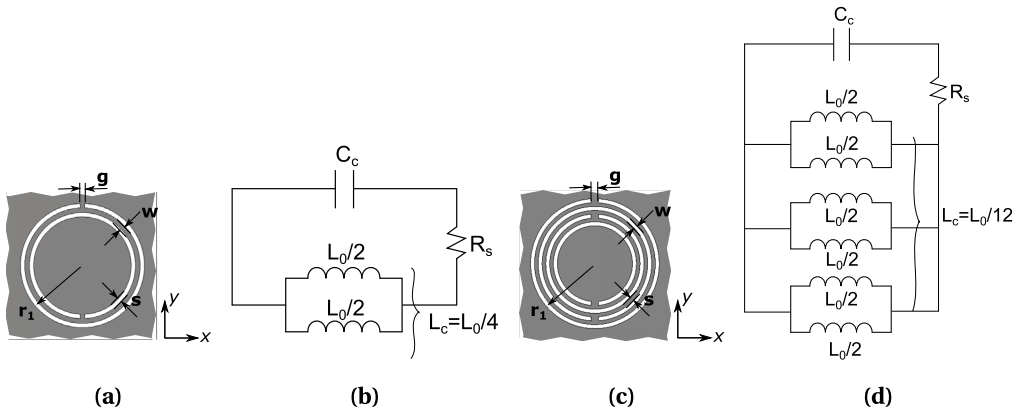

Figure 2. (a) Sketch of the CSRR unit cell geometry, $n = 2$, (all the dimensions are in mm): $w = s = 1$; $r_1 = 13.1$; $g = 1$. (b) Circuit model of the CSRR. Values are computed as in (1): $L_c = 2.06$ nH, $C_c = 5.62$ pF, $R_s = 0$ (lossless case). (c) Geometry of the MCSRR unit cell, for $n = 4$, re-tuned to resonate at 1.5 GHz. $w = 0.78$; $r_1 = 10$; $g = 1$; $s = 0.35$. (d) Circuit model of the MCSRR. Circuit quantities are: $L_c = 2.63$ nH, $C_c = 4.58$ pF.

where f_0 is the resonant frequency, C_c is the capacitance of a conductor disk surrounded by a ground plate, L_0 is the inductance connecting such disk to ground from two sides. For duality, the parameter $C_{0,\mathrm{SRR}}$, which represents the total capacitance between the conductor strips in the equivalent SRR, is used to compute L_0. In the same way, the total inductance of the SRR, L_S, is used to estimate the capacitance C_c in the CSRR. This approximations are valid for the lossless case. Higher order effects like mutual inductances, the mutual capacitances between non adjacent slots and the split inductance are neglected in the model [15]. The exact solution for L_s for the conventional SRR is presented in [17]. An approximate model for the total inductance L_C in the MCSRR case is described in [15].

The narrowband response of both, the CSRR- and the MCSRR-FSS showing its bandpass filter capability is observed in Figure 3, where each unit cell has been simulated as a periodic lattice to form and ideally infinite FSS. Only waves whose E-field is aligned to the gaps in the rings (y-axis in Figure 2a) will be able to pass through the FSS, at frequencies slightly higher than the resonant frequencies of the composing CSRR sizes. The 3 dB-bandwidth of the passband around f_0 is 35 MHz (2.33%), for the CSRR and 4.6 MHz (0.31%) for the MCSRR case. The Q-factor, $Q = f_0/BW_{3\ \mathrm{dB}}$, yields 42.8 for the CSRR and 328 for the MCSRR. The improvement in the selectivity of the passband response is evident for the MCSRR.

Since the increase in the Q-factor comes with a miniaturization effect, represented by a resonant frequency shift to lower frequencies, a re-tuning of the geometrical parameters of the MCSRR was needed to compare both FSS's at the same frequency, $f_0 = 1.475$ GHz. The final dimensions are described in the caption of Figure 2. A more detailed analysis of multiple turns ring resonators and spiral resonators is presented in [15]. The resulting radiated electric field waveform is presented in Section 3.

2.2. *Multiband single layer FSS*

The proposed unit cell is to be supported by a low relative permittivity substrate, (ideally $\epsilon_r = 1$), simulated as losses free as a first approximation. It is composed of two different CSRRs, oriented as shown in Figure 4a. Since the intended response of the FSS is multiband, each band shall be

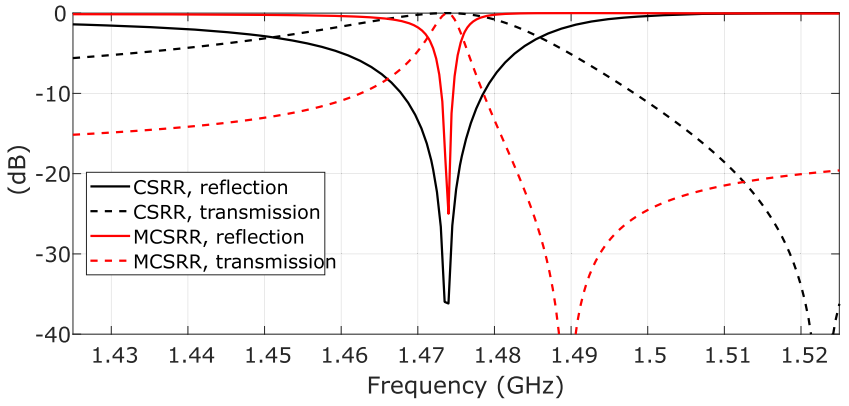

Figure 3. Reflection and transmission parameters for the CSRR and the MCSRR FSS's. The improvement in the Q-factor is evident for the MCSRR ($n = 4$).

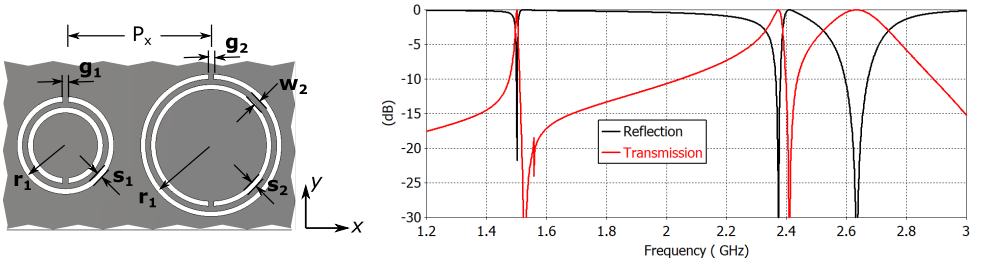

(a) **(b)**

Figure 4. (a) Sketch of the two CSRR unit cells geometry. Unit cell 1, on the left, is associated with a passband frequency of 2.4 GHz. The unit cell on the right is resonant at 1.5 GHz. The dimensions are (all in mm) $P_x = 26.5$, $P_y = 26.5$, $r_1 = 8.5$, $r_2 = 12.65$, $g_1 = g_2 = 1$, $s_1 = s_2 = 1$, $w_1 = w_2 = 1$, and (b) FSS response, simulated as an infinite periodic structure.

tuned according to the resonant frequency of each unit-cell size. Figure 4b shows the reflection and the transmission parameter, respectively, for the CSRR-based FSS. An additional resonant frequency is observed at 2.6 GHz in Figure 4b. This is associated with a high-frequency resonance of the 1.5 GHz unit cell. This additional passband is expected to be overlapped with the response from the 2.4 GHz unit cell.

3. HPM radiator integration

3.1. *Reflector based IRA*

The sketch of a two-arm IRA is shown in Figure 5a. When connected to a pulsed voltage source, the IRA radiates an impulse-like waveform over a narrow beam on boresight direction (z-axis in Figure 5a). The electric field related to the waveform radiated by the IRA can be described as [18]:

$$E_t(t,r) = f_1 \frac{1}{2\pi f_g} \left(\begin{array}{c} \dfrac{V(t-r/c)}{r} \dfrac{\sin(\beta)}{1+\cos(\beta)} - \dfrac{V(t-L/c-R_2/c)}{R_2} \dfrac{\sin(\beta)+\sin(\gamma)}{1+\cos(\beta-\gamma)} \cdots \\ -\dfrac{4}{D} V(t-2F/c-r/c) + (2+2\cos(\gamma)) \dfrac{V(t-l/c-R_2/c)}{D} \end{array} \right) \left(\frac{V}{m}\right) \qquad (2)$$

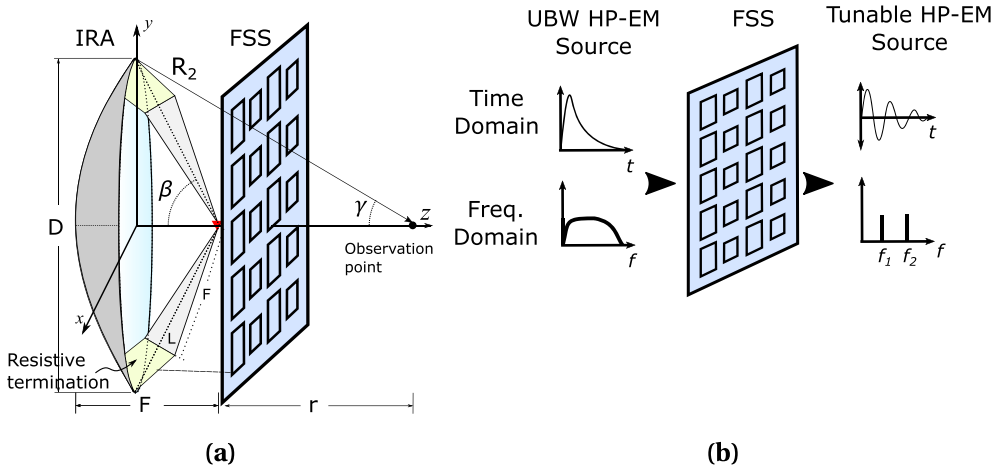

Figure 5. (a) IRA + FSS geometry, and (b) principle of the Tunable HPM Radiator.

where $V(t)$ is the feeding voltage, $f_1 = 1$ for the two-arm IRA, c is the speed of light, and r is the distance between the focal point and the measurement point. The geometric impedance factor, $f_g = Z_{\text{IRA}}/120\pi$, is a reference parameter related to the feeder geometry which acts as the transmission line of the spherical wave into the reflector. Z_{IRA} is the input impedance of the antenna. D, F, l, β, γ, and R_2 are described in Figure 5a. The two-arm IRA presented in this paper is designed with the following parameters: $D = 1$ (m), $F/D = 0.4$, $Z_{\text{IRA}} = 400$ (Ω).

3.2. *Tunable HPM radiator with FSS*

The multiband radiator concept presented here is depicted in Figure 5b. The FSS acts as a pass-band filter with a high-Q factor response. As mentioned before, the FSS modifies the impulse-like waveform propagating from the IRA by converting it into a damped sinusoidal. For the case of the multiband FSS, the radiated waveform will present two main frequency components. Only the electric field components aligned with the y-axis, and around the resonant frequency of each unit cell, will effectively pass through the FSS. Unit cells of the same size are aligned along the y-axis, in order to align each resonant polarization with the incoming wideband transient wave from the IRA.

One effective way of determining the radiated electric field waveform, from the IRA + FSS system, is by applying classical linear cascaded system approach, as outlined in Figure 1.

The field radiated from the IRA in (2) can be related to the voltage at the feed point through the transfer function, $T_A(f)$, computed as

$$T_A(f) = E_{\text{IRA}}(f)/V_{\text{IN}}(f). \tag{3}$$

$T_A(f)$ can be understood as the inverse of the effective length, $l_{\text{eff}(f)}$ of the IRA. Note that the $E_{\text{IRA}}(f)$ does not necessarily have to be computed in the far-field region. Due to the nature of the radiation from a parabolic reflector, a normally incident E field propagates through the FSS from the left (see Figure 5b), and continues along the z-axis, but with its spectral characteristics filtered.

By applying the chain parameters approach, as described in [5], it is possible to represent the FSS by a linear two-port network. The conventional currents and voltages are linearly related to

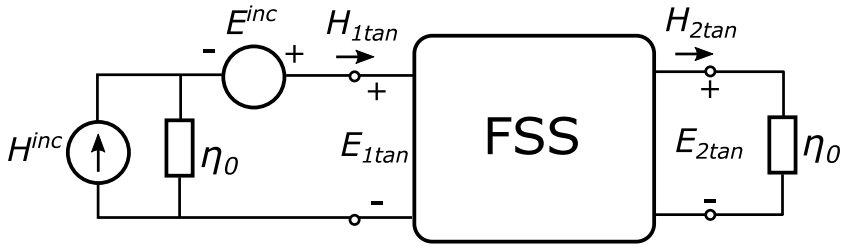

Figure 6. FSS, as an $ABCD$ parameter circuit representation. Tangential E- and H-field act as the voltage and current variables of a conventional circuit model. The FSS in this paper replaces the conductive grid representation in [5].

the tangential components of the E- and H-fields at the input and output ports, as depicted in Figure 6. This yields to

$$\begin{bmatrix} E_{1,\tan} \\ H_{1,\tan} \end{bmatrix} = \begin{bmatrix} A & B \\ C & D \end{bmatrix} \begin{bmatrix} E_{2,\tan} \\ H_{2,\tan} \end{bmatrix}. \tag{4}$$

The tangential fields $E_{1,2}$, and $H_{1,2}$ represent the network input and output voltages, $V_{1,2}$, and currents $I_{1,2}$, respectively, of a terminated two-port network. By using the expression for the current in the load (see [19], ch. 3), the same expression gives the voltage (or current) transfer function, as the ratio of $V_2(f)/V_1(f)$. The current through the load, represented by $H_{2,\tan}$, can be computed as

$$\begin{aligned} H_{2,\tan} &= \frac{E_{2,\tan}}{\eta_0} = \frac{E^{\text{inc}}}{(A+\eta_0 C)\eta_0 + (B+\eta_0 D)} \\ E^{\text{inc}} &= 2E_{1,\tan} \end{aligned} \tag{5}$$

where η_0 is the free space impedance (i.e., 377 Ω).

Then, the transfer function of the FSS can be easily computed from the transmission-reflection parameters shown in Figure 3. In this model, $E_{1,\tan}(f) = E_{\text{IRA}}(f)$. The output tangential $E_{\text{IRA+FSS}}(f)$, in the y-axis direction, can be computed as

$$\begin{aligned} E_{\text{IRA+FSS}}(f) &= E_{2,\tan} = 2E_{1,\tan}\left(\frac{\eta_0}{(A+\eta_0 C)\eta_0 + (B+\eta_0 D)}\right) \\ E_{\text{IRA+FSS}}(f) &= T_{\text{FSS}} E_{1,\tan}. \end{aligned} \tag{6}$$

Finally, an expression for the electric field once the transient pulse passes through the FSS is given by

$$\begin{aligned} T_{\text{TOTAL}}(f) &= T_A(f)\, T_{\text{FSS}}(f) \\ E_{\text{IRA+FSS}}(f) &= T_{\text{TOTAL}} V_{\text{IN}}(f). \end{aligned} \tag{7}$$

Once the complete transfer function of the integrated IRA + FSS radiator is extracted, the spectral response of the electric field waveform, related to a pulsed voltage signal driving the IRA terminals, i.e., $V_{\text{IN}}(f)$, can be analytically evaluated, as it will be shown below. The electric field in the time domain can be computed as the inverse Fourier transform of $E_{\text{IRA+FSS}}(f)$.

3.3. *Results*

The integrated FSS + IRA radiator is modeled in the commercial suite CST. A square array of unit cells is designed to cover 1 m^2, which is the area circumscribing the reflector aperture. In both FSS typologies we are illustrating, the FSS structure is located 10 cm away from the focal point of the IRA. Although a larger separation between FSS and antenna would minimize multiple reflections, diffracted waves from the perimeter of the FSS structure will have a more significant effect in the filtered pulse.

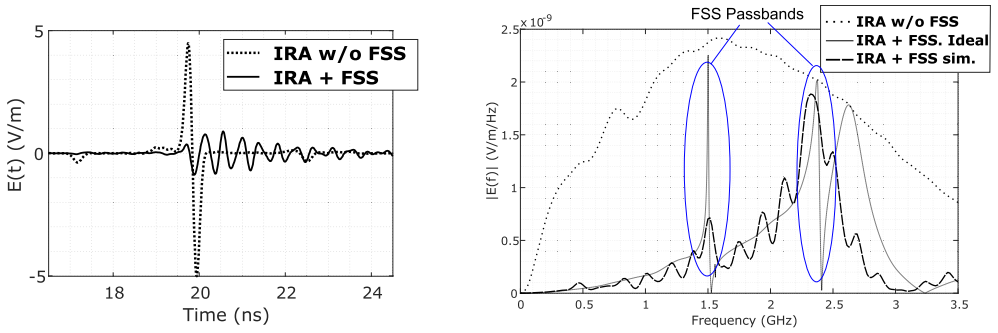

(a) **(b)**

Figure 7. (a) Electric field in the time domain, 5 m away from the focal point of the IRA. (b) Spectral amplitude of the IRA + FSS.

The multiband FSS is designed as an array of 22×36 unit cells (see Figure 4a). The whole system, IRA + FSS, is discretized into a 50 million cells mesh, applying a electric symmetry around the xz-plane (see Figure 5b). An absorbing open boundary was set quarter-wavelength (at 1.5 GHz) away from the structure. 19,600 time steps were simulated with a time-step length of 7.6×10^{-4} ns. The cell fraction at maximum frequency was set to 20. The simulation time reached 2 h in a computer with a GPU of 512 cores and 6 GB memory size. The electric field has been computed 5 m away from the focal point of the IRA, in broadside (z-axis). The time-domain response of the radiated electric field is shown in Figure 7a. The field radiated by a conventional two-arm unloaded IRA, with the same dimensions, is also shown as a reference. In both cases, a Gaussian pulse, with spectral content ranging from 0 to 3.5 GHz and 18 V in amplitude in the time domain, is used as the driving signal. The damped-like sinusoidal response of the proposed design is observed, as expected.

The passband filtering behavior of the FSS loading the IRA is observed in the frequency domain response of the electric field, as shown in Figure 7b. The ideal filtering response of the IRA + FSS system can also be computed by applying the chain parameter analysis described by (4)–(7), and is shown as a reference. For the ideal system response, the ABCD parameters of the FSS have been computed from the single unit cell simulation in Figure 4b, using the infinite periodic boundary conditions capability of the simulator. This leads to a significantly shorter simulation time since the IRA is simulated apart from the FSS.

Despite the amplitude drop in the full-wave simulated IRA + FSS field, the intended passband effect holds around the resonant frequency of each unit-cell size, as can be seen in Figure 7b. Ideally, the impulse-like radiated pulse shall be converted into a signal with two different frequency components. However, harmonic resonances from the unit cells limit the bandwidth operation of the integrated radiator, as observed in the overlapped band around 2.6 GHz.

A symmetric and still directive radiation pattern can be expected, since the structure symmetry of the original IRA is not affected by adding the FSS, as it is shown in Figure 8. Significant degradation in the SLL ratio is observed in both frequency bands, especially in the E-plane. The effects of diffraction due to the FSS edges are evident but less severe at higher frequencies (i.e. 2.4 GHz). The maximum directivity is decreased from 18 dBi to 11 dBi at 1.5 GHz, while remained 22 dBi at 2.4 GHz (see Figure 8). This response is in accordance with the higher field strength around 2.4 GHz, once the wave passes through the FSS (see Figure 7b). One possible solution for this problem can be simply increasing the total area of the FSS, at the expense of affecting the manageability of the radiator. Furthermore, the reduced radiation intensity on boresight at the lower frequency band, could also be associated with the electrical size of the simulated

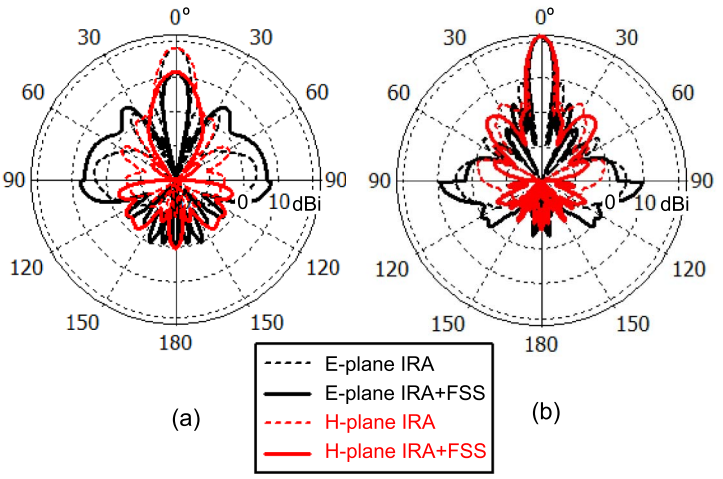

Figure 8. Radiation response of the integrated radiator, IRA + FSS (a) 1.5 GHz, and (b) 2.4 GHz. The radiation pattern from the unloaded IRA is shown as a reference.

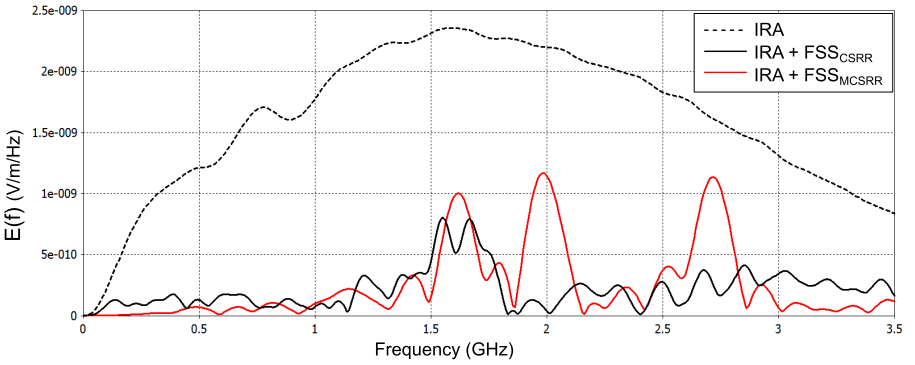

Figure 9. Spectral amplitude of the electric field amplitude, computed 5 m away from the Integrated HPM radiator, for both the CSRR- and the MCSRR-based FSS.

structure (1×1 m^2). Experimental validation is therefore required to confirm the influence of the finite-size FSS on the radiation diagram of the overall system.

The radiated field on boresight is computed for the MCSRR-based FSS. The numerical simulation is presented in Figure 9. Besides the drop in amplitude in the passing band in both, the CSRR- and the MCSRR-based FSS, the increase in the Q-factor is observed for the MCSRR case. Multiple bands for the MCSRR are observed as expected, due to the multiple coupling between the increased number of turns in the unit cell. In general, the resulting combination of the FSS with the IRA provides an efficient way to introduce the tunability and agility for multiple applications of the HPM source.

4. Conclusion

The concept of designing a narrowband HPM radiator is presented as the integration of a passband FSS with high Q-factor capabilities. An analytical approach to compute the radiated electric field is presented along with the fullwave simulation for validation. An enhanced FSS,

in terms of passband selectivity, is presented by implementing the axial-symmetric multiple-CSRR as unit cell. Computed results in terms of the field strength, spectral density of the electric field, and the radiation pattern of the integrated antenna system have been obtained. The presented approach is also applicable to other FSS geometries and UWB radiators. Currently, the implementation of a prototype of the proposed design is under process for experimental validation.

References

[1] D. D. V. Giri, F. M. Tesche, "Modeling of propagation losses in common residential and commercial building walls", 2013, http://ece-research.unm.edu/summa/notes/In/IN624.pdf, *Interaction Notes* 624, 24 pages, published by the Summa Foundation.

[2] D. V. Giri, R. Hoad, F. Sabath, "Implications of high-power electromagnetic (HPEM) environments on electronics", *IEEE Electromagn. Compat. Mag.* **9** (2020), no. 2, p. 37-44.

[3] C. E. Baum, "Radiation of impulse-like transient fields", 1989, http://ece-research.unm.edu/summa/notes/SSN/note321.pdf, *Sensor and Simulation Notes* 321, 28 pages, published by the Summma Foundation.

[4] C. E. Baum, E. G. Farr, "Impulse radiating antennas", in *Ultra-Wideband, Short-Pulse Electromagnetics* (H. L. Bertoni, L. Carin, L. B. Felsen, eds.), vol. 2, Springer US, Boston, MA, 1993, p. 139-147.

[5] F. M. Tesche, D. V. Giri, "Modification of impulse-radiating antenna waveforms for infrastructure element testing", 2015, http://ece-research.unm.edu/summa/notes/SSN/SSN572.pdf, *Sensor and Simulation Notes* 572, 25 pages, published by the Summa Foundation.

[6] W. Bigelow, E. Farr, J. S. Tyo, "A frequency selective surface used as a broadband filter to pass low-frequency UWB while reflecting X-band radar", 2006, http://www.farr-research.com/Papers/ssn506.pdf, *Sensor and Simulation Notes* 506, 17 pages, published by the Summa Foundation.

[7] C. Yang, P.-G. Liu, X.-J. Huang, "A novel method of energy selective surface for adaptive HPM/EMP protection", *IEEE Antennas Wirel. Propag. Lett.* **12** (2013), p. 112-115.

[8] S. Monni, D. J. Bekers, M. van Wanum, R. van Dijk, A. Neto, G. Gerini, F. E. van Vliet, "Limiting frequency selective surfaces", in *2009 European Microwave Conference (EuMC)*, IEEE, 2009, p. 606-609.

[9] M. Mavridou, K. Konstantinidis, A. Feresidis, P. Gardner, "Novel tunable frequency selective meta-surfaces", in *2016 46th European Microwave Conference (EuMC)*, IEEE, 2016, p. 301-304.

[10] D. Li, T. Li, E. Li, Y. Zhang, "A 2.5-D angularly stable frequency selective surface using via-based structure for 5G EMI shielding", *IEEE Trans. Electromagn. Compat.* **60** (2017), no. 3, p. 768-775.

[11] B. A. Munk, *Frequency Selective Surfaces: Theory and Design*, John Wiley & Sons, New York, 2005.

[12] J. B. Pendry, A. J. Holden, D. J. Robbins, W. J. Stewart, "Magnetism from conductors and enhanced nonlinear phenomena", *IEEE Trans. Microw. Theory Techniq.* **47** (1999), no. 11, p. 2075-2084.

[13] R. Marqués, J. D. Baena, M. Beruete, F. Falcone, T. Lopetegi, M. Sorolla, F. Martín, J. Garcia, "Ab initio analysis of frequency selective surfaces based on conventional and complementary split ring resonators", *J. Opt. A: Pure Appl. Opt.* **7** (2005), no. 2, p. S38-S43.

[14] J. D. Ortiz, J. D. Baena, V. Losada, F. Medina, J. L. Araque, "Spatial angular filtering by FSSs made of chains of interconnected SRRs and CSRRs", *IEEE Microw. Wirel. Compon. Lett.* **23** (2013), no. 9, p. 477-479.

[15] F. Bilotti, A. Toscano, L. Vegni, "Design of spiral and multiple split-ring resonators for the realization of miniaturized metamaterial samples", *IEEE Trans. Antennas Propag.* **55** (2007), no. 8, p. 2258-2267.

[16] J. D. Baena, J. Bonache, F. Martin, R. M. Sillero, F. Falcone, T. Lopetegi, M. A. G. Laso, J. Garcia-Garcia, I. Gil, M. F. Portillo, M. Sorolla, "Equivalent-circuit models for split-ring resonators and complementary split-ring resonators coupled to planar transmission lines", *IEEE Trans. Microw. Theory Techniq.* **53** (2005), no. 4, p. 1451-1461.

[17] R. Marques, F. Mesa, J. Martel, F. Medina, "Comparative analysis of edge- and broadside-coupled split ring resonators for metamaterial design—theory and experiments", *IEEE Trans. Antennas Propag.* **51** (2003), no. 10, p. 2572-2581.

[18] O. V. Mikheev, S. A. Podosenov, K. Y. Sakharov, A. A. Sokolov, Y. G. Svekis, V. A. Turkin, "New method for calculating pulse radiation from an antenna with a reflector", *IEEE Trans. Electromagn. Compat.* **39** (1997), no. 1, p. 48-54.

[19] F. M. Tesche, M. Ianoz, T. Karlsson, *EMC Analysis Methods and Computational Models*, John Wiley & Sons, New York, 1996.